Very-small angle neutron scattering study on grain coarsening inhibition by V-doping of WC-Co composites

N.B. When citing this work, cite the original published paper.

(article starts on next page)

Very-small angle neutron scattering study on grain coarsening inhibition by V-doping of WC-Co composites

Ahmet Bahadir Yildiz [a,*], Jonathan Weidow [b], Vasyl Ryukhtin [c], Susanne Norgren [d,e], Göran Wahnström [b], Peter Hedström [a]

[a] Department of Materials Science and Engineering, KTH Royal Institute of Technology, SE-100 44 Stockholm, Sweden
[b] Department of Physics, Chalmers University of Technology, SE-412 96 Göteborg, Sweden
[c] Nuclear Physics Institute, 250 68, cp. 130, Husinec-Řež, Czech Republic
[d] Sandvik, SE-126 80 Stockholm, Sweden
[e] Department of Engineering Sciences, Applied Materials Science, Uppsala University, SE-751 21 Uppsala, Sweden

ARTICLE INFO

ABSTRACT

The mechanical properties of cemented carbides can be tuned by controlling WC grain coarsening and the simultaneous growth of the binder pocket size during the sintering. So far, bulk studies considering this phenomenon are scarce, but here, we report the first very-small angle neutron scattering (VSANS) study on cemented carbides. VSANS is supplemented with electron backscatter diffraction (EBSD) and the microstructural refinement by increasing V-doping (0, 0.02, 0.22, and 0.76 wt%) is quantified. The capability of VSANS as a non-destructive bulk probe for cemented carbides is shown, paving way for forthcoming in-situ studies.

© 2019 Acta Materialia Inc. Published by Elsevier Ltd. This is an open access article under the CC BY license (http://creativecommons.org/licenses/by/4.0/).

Cemented carbides are composite materials manufactured via liquid-phase sintering. Their excellent wear resistance, high hardness, and high toughness make them widely used as, for example, metal cutting tools. The performance of traditional cemented carbide tools relies on the as-sintered composite microstructure consisting of hard tungsten carbide (WC) grains embedded in a ductile Co-based binder phase. The Co-based binder forms a liquid phase during the sintering. This facilitates diffusion and effective densification of the powder mixture, but it also leads to coarsening of the WC grains, and correspondingly the size of the binder regions between the WC grains, hereinafter referred to as the binder pocket size, increases [1].

Fine-grained cemented carbides are in demand for cutting applications requiring high hardness and sharp cutting edges [2–4]. For a constant binder phase fraction, the hardness of the cemented carbide increases with decreasing WC grain size and Co-based binder free-path [5–7]; however, this occurs at the expense of the fracture toughness [8]. The accurate determination of the binder pocket size and WC grain size is thus critical for relating the microstructure and the mechanical properties in cemented carbides.

During the last two decades, electron backscatter diffraction (EBSD) has emerged as the tool of choice for grain size determinations in cemented carbides. EBSD is an effective method, but some limitations are, for example, the demanding sample preparation and limited spatial resolution, in particular when fine-grained cemented carbides are analyzed [9]. Another limitation is that it is a sectioning technique limited to 2D observations. A technique enabling 3D size determinations would be preferred, for example, when calibrating models for grain coarsening [10,11], but more importantly a tool to characterize grain coarsening in-situ would be preferred.

Small angle scattering (SAS) techniques have been shown useful for non-destructive 3D bulk characterization of particles, i.e. nano-scale precipitates, in earlier works on alloys [12,13]. By extending the detection of scattering vectors to even smaller angles using very- or ultra-SAS technique, the characterization of microstructural features up to several μm in size is enabled [14–16]. However, the poor penetration of X-ray beams in materials made of heavy elements such as W and Co, makes ultra- or very-small angle neutron scattering (USANS or VSANS) the only viable SAS techniques for the investigations of binder pocket size and WC grain size in cemented carbides as bulk materials. Non-destructive bulk characterization using USANS/VSANS would have the added benefit of in-situ capabilities during the sintering process.

Motivated by both the potential use of VSANS for in-situ characterization of the microstructure in cemented carbides, and the need for

* Corresponding author at: Department of Materials Science and Engineering, KTH Royal Institute of Technology, Sweden.
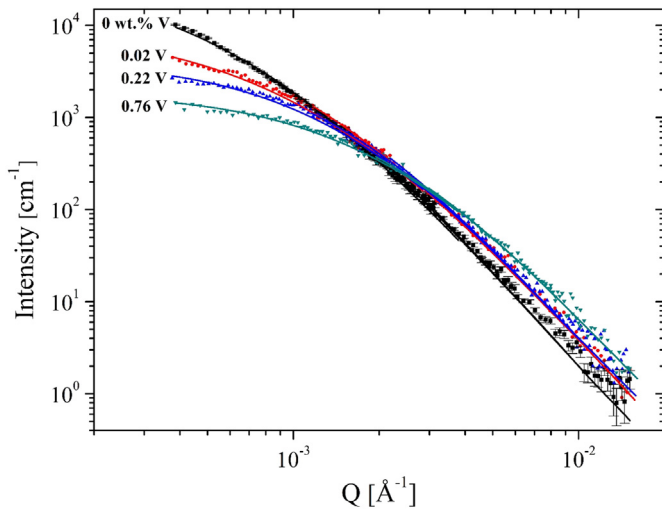E-mail address: abyildiz@kth.se (A.B. Yildiz).

Fig. 1. The evolution of VSANS curves log-log scale as a function of V addition in WC-Co-Vx (x = 0 to 0.76 wt% V) cemented carbides. The solid lines correspond to the model fit. Note that, except for 0 wt% V sample, error bars are omitted for clarity as they obscure the data.

better insights in microstructural refinement due to V-doping, we here investigate the evolution of Co-based binder pocket size in WC-Co-V cemented carbides using VSANS. We report on the first investigation of WC-Co cemented carbides using VSANS, and it provides a feasibility test for forthcoming *in-situ* studies. EBSD was used to supplement the VSANS data and an empirical expression is presented to estimate the average WC grain size.

One WC-11.45 wt% Co composite and three WC-10.07 wt% Co composites with different V contents (0.02, 0.22, and 0.76 wt%) were investigated. WC powder from Wolfram Bergbau Hütten AG with an average diameter of 0.9 μm (Fisher Sub-Sieve Sizer [17]) was used for the hard phase, Co powder from Freeport for the binder, and V was added as VC from Treibacher AG. The powders were mixed with ethanol and Polyethylene glycol and milled for 8 h in a 0.25 L rotating mill (lined with WC-Co) using 900 g of pure WC-Co milling bodies to avoid contamination. Thereafter, the ethanol was removed by pan drying at 40 °C in N_2 atmosphere. The powder was uniaxially pressed into inserts with ISO-SNUN square geometry (12.7 mm × 12.7 mm × 4.2 mm), sintered in controlled vacuum at 1410 °C for 1 h, cooled to 1250 °C using a cooling rate of 5 °C/min, and finally furnace cooled to room temperature. The use of the same initial powder as well as milling and sintering procedures ensure the similar particle size distribution prior to the sintering and makes the amount of V-doping the single dominant parameter affecting the WC grain coarsening.

Ex-situ VSANS experiments were performed on the double-bent-crystal diffractometer MAUD [18] at Nuclear Physics Institute (NPI), Czech Republic, to probe the evolution of the microstructural features. VSANS data were acquired at three different instrumental resolutions – high, low and medium. Desired instrumental resolutions were set by bending of the analyzer and monochromator crystals. This experimental setup spanned a scattering vector (Q) range of $0.00031 < Q < 0.02$ Å^{-1} ($Q = (4\pi/\lambda) \sin\theta$, where θ is half of the scattering angle) at a constant incident neutron wavelength of 2.09 Å. This Q-range corresponds to scattering features with sizes from about 30 nm up to 2 μm in real space. For VSANS experiments, square specimens with a dimension of 12 mm × 12 mm were cut. In order to minimize multiple scattering and keep high transmission (> 90%), the specimen thickness was limited to 0.35 mm. To reduce the scattering caused by the magnetic domain walls in Co, specimens were horizontally placed between two Neodymium magnets, providing a magnetic field of about 0.5 T perpendicular to the neutron beam. The measured VSANS data were corrected for sample-independent background using measurements of Cd,

normalized by the transmission and scaled to absolute units by using the probe volume.

EBSD samples were prepared by first cutting of 300 μm slices using a high-speed saw. The samples were thereafter polished manually with polycrystalline diamond spray with the last step being performed using 1 μm diamonds. The specimens were further polished by Ar$^+$ ions for two hours in a Gatan Precision Ion Polishing System Model 691. Both guns were used continuously at 4.0 kV at an incidence angle of 2°. The EBSD measurements were conducted at 20 kV acceleration voltage using 50 nm step size in a Tescan GAIA3 focused ion beam scanning electron microscope (SEM) equipped with an Oxford Instruments NordlysNano camera. The Oxford Instruments software packages AZtecHKL and Tango were used for the post-processing and analyses. A misorientation threshold angle of 3° was set to define the grains; the minimum grain size considered was 4 pixels. EBSD images of WC grains were generated using the MTEX software package [19].

The presence of compositional inhomogeneities such as precipitates, segregation, and porosity can cause local differences in the scattering length density (SLD). In SANS experiments, this difference results in a scattering signal at a certain scattering vector Q related to the size of the scatterers, D, ($Q \approx 2\pi/D$). In the V-doped WC-Co material, within the VSANS Q-range, the scattering can result from: (i) the SLD difference between the Co-based binder pockets and the WC grains; (ii) porosity; and (iii) the SLD difference caused by bulk (V,W)C precipitates. Backscattered SEM images and energy dispersive x-ray spectroscopy (EDS) composition maps, not presented here, revealed no bulk (V,W)C precipitates in the samples containing 0.02% and 0.22% V addition. However, for the sample containing 0.76% V, V enriched regions up to 2 μm in size have been observed, indicating bulk (V,W)C precipitates. The additional scattering arising from the potential (V,W)C precipitates is judged to be minor considering the low potential fraction of (V,W)C. Furthermore, for $(V_{0.92}, W_{0.08})C_{0.8}$ [20] (SLD$_{(V,W)C}$ = 3.78 × 10^{-6} Å^{-2}), a lower SLD difference with respect to pure Co (SLD$_{Co}$ = 2.26 × 10^{-6} Å^{-2}) is expected compared to WC (SLD$_{WC}$ = 5.48 × 10^{-6} Å^{-2}). The samples also have over 99.5% relative density after sintering, indicating fully consolidated composites. Therefore, in the current study, the VSANS data originate mainly from the SLD difference between the Co-based binder and the WC grains. Fig. 1 shows the evolution of VSANS intensities as a function of V addition. The scattering curves at low-Q obey Guinier law, whilst at high-Q Porod scattering is found. Upon V-doping, two different trends occur in the scattering intensities. With increasing V content, VSANS intensity decreases at low-Q region ($Q < 0.002$ Å^{-1}), and conversely increases at the high-Q region. These development trends
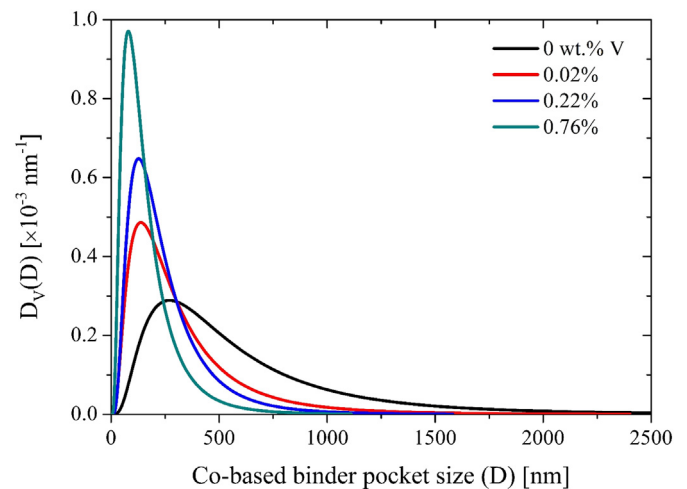

Fig. 2. The volume-weighted size distribution $D_V(D)$ of Co-based binder pockets in WC-Co-Vx (x = 0 to 0.76 wt% V) cemented carbides calculated by VSANS using indirect Fourier transformation method.
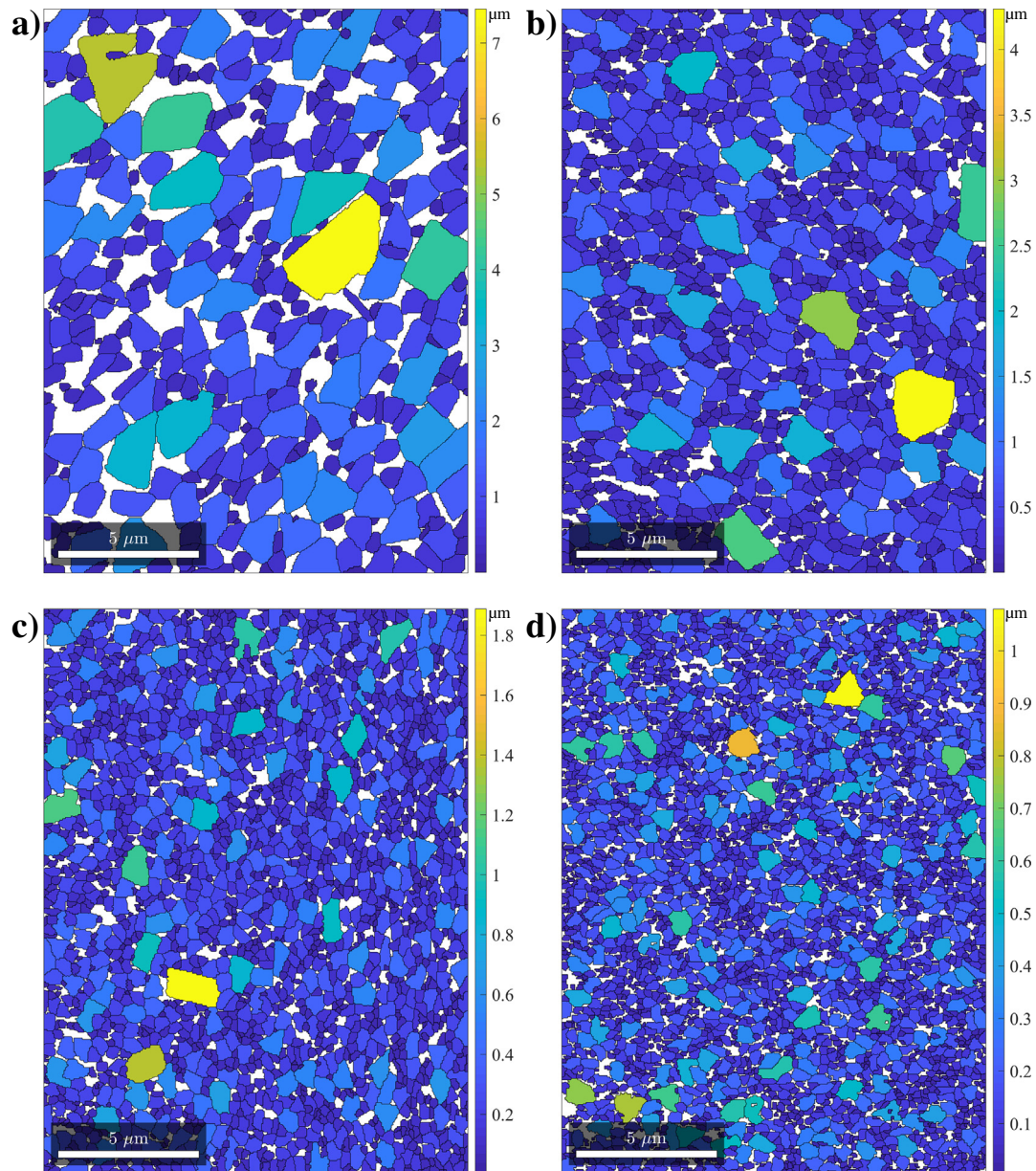
Fig. 3. Colored EBSD maps showing the size distribution of WC grains in a) 0%, b) 0.02%, c) 0.22%, and d) 0.76 wt% V-doped WC-Co cemented carbides. The grain boundaries represented by black lines is defined by a misorientation >3°. Note the rescaling of the color bar between the images. (For interpretation of the references to color in this figure legend, the reader is referred to the web version of this article.)

in the scattering data indicate a microstructural refinement due to the V addition.

In order to determine the average binder pocket size and their distribution, the VSANS curves were fitted in the SASProFit [21] software package using indirect Fourier transformation method [22] with slit-smeared scattering geometry. The complex microstructure with polydispersity and irregular morphology of the binder regions were modelled using an assumption of log-normal distribution of spherical particles. As it is explained in Ref. [21], this simple shape assumption can statistically describe the microstructural evolution in terms of size and size distribution. The possible compositional changes in the Co-based binder due to the C activity and the V addition [23] could not only affect the nuclear SLD of Co but also cause differences in the residual magnetic scattering. Since the initial composition of the powder mixture is known, the volume fraction of binder phase at 900 °C [24], the temperature below which the compositional changes are small [25], was estimated by Thermo-Calc Software [26] TCFE9 Steels/Fe-

alloys database and the calculated binder volume fractions were used as a fixed parameter in the fitting procedures. This allows the usage of SLD difference as a free parameter, which now stands for a scattering power originated from the nuclear scattering and residual magnetic scattering. The solid lines in Fig. 1 represent the model fit of the VSANS curves.

Fig. 2 shows the evolution in the size distribution of binder pockets as a function of V addition. It should be noted that $D_V(D)$ denotes the volume-weighted size distribution function for the binder phase. Thus, the integration of $D_V(D)$ gives the volume fraction of the binder phase, which ranges between 17.3 and 19.3 vol%. As can be seen, an increasing amount of V-doping results in: (i) a shift in the maximum of size distribution towards smaller values; (ii) a narrower size distribution; and (iii) an increased intensity of distribution peak height. Correspondingly, the average size of the binder pockets reduces gradually from 626 ± 14 nm to 169 ± 7 nm in 0% V and 0.76% V samples, respectively. Since the refinement in WC grain size takes place together with refinement
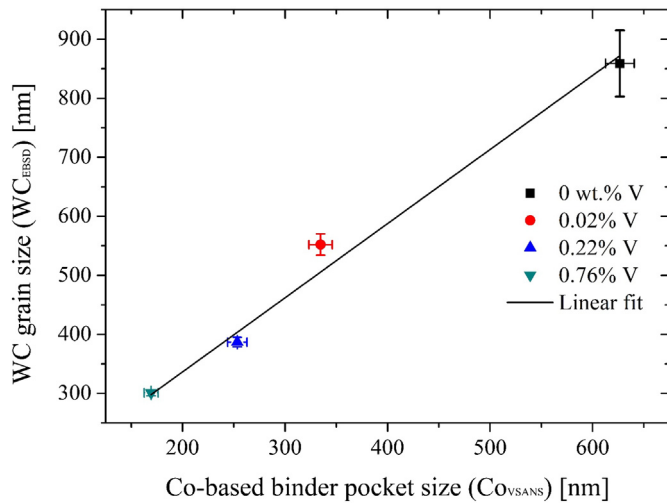
Fig. 4. The average WC grain size measured by EBSD (WC_{EBSD}) *versus* Co-based binder pocket size measured by VSANS (Co_{VSANS}) in WC-Co-Vx (x = 0 to 0.76 wt% V) cemented carbides. The solid line is the linear fit. Scatter bars in WC_{EBSD} and Co_{VSANS} values represent the 95% confidence interval calculated according to Ref. [30] and standard deviations from the model fitting, respectively.

in binder pocket size, the reduction in the average binder pocket size is attributed to the presence of smaller WC grains due to the V addition.

EBSD maps colored according to grain size, *i.e.* equivalent circle diameter, are presented in Fig. 3. Only a few grains were viewed normal to the basal plane. In accordance with the previous work [11,27], the majority of the WC grains had an irregular shape. It can be seen that a strong refinement in grain size was observed already after a minor V addition (0.02%), which was followed by a gradual decrease. EBSD results showed that upon adding V, the average WC grain size decreased from 859 ± 56 nm (0% V) to 301 ± 5 nm (0.76% V).

For a constant binder phase fraction, WC grain size is proportional to the mean free path of binder phase that reduces with the refinement in WC grain size [4]. Therefore, the evolution of the mean free path of the binder phase can also be used as an indirect measure of the WC grain size refinement, and empirical expressions can be defined for the estimation of WC grain size [1,28,29]. Fig. 4 plots the average size evolutions in WC grains measured by EBSD (WC_{EBSD}) and Co-based binder pockets measured by VSANS (Co_{VSANS}). As can be seen, a linear relationship is found between WC_{EBSD} and Co_{VSANS}, which is consistent with the previous literature findings [1,4,29]. The linear fit gives the following empirical relation:

$$WC_{EBSD} = 1.2(\pm0.1) \times Co_{VSANS} + 85.3(\pm35.9) \text{ [nm]} \quad R^2 = 0.94$$

which could give a reasonable approximation of WC grain size in WC-Co cemented carbides with approximately 10 wt% Co. However, further work would be needed to improve such relations for the materials systems containing various amount of binder phase and other binder materials.

In conclusion, we have performed *ex-situ* VSANS experiments to study the evolution of Co-based binder pocket size distribution in WC-Co-V (from 0 to 0.76 wt% V) cemented carbides. The addition of V results in a decrease in the VSANS intensity at low-Q and increase at high-Q regions of the scattering curves, which imply a microstructural refinement upon V-doping. Modeling of VSANS data reveals that V

addition results in smaller binder pockets with narrower size distribution. Supplementary EBSD results also confirm a refinement in the WC grain size. We find a linear relationship between the average binder pocket size measured by VSANS and WC grain size measured by EBSD and present an empirical relation to estimate the WC grain size. Hence, our results indicate great potential for utilization of VSANS for bulk characterization of WC grain coarsening in cemented carbides, where the non-destructive *in-situ* capability should be explored.

References

[1] B. Roebuck, E.G. Bennett, Metallography 19 (1986) 27–47.
[2] W.D. Schubert, H. Neumeister, G. Kinger, B. Lux, Int. J. Refract. Met. Hard Mater. 16 (1998) 133–142.
[3] A. Grearson, M. James, M. Tillman, S. Norgren, P. Gustafson, Proc. 16th Int. Plansee Semin. Refract. Hard Mater, Plansee Metall AG, Austria, 2005.
[4] J. García, V.C. Ciprés, A. Blomqvist, B. Kaplan, Int. J. Refract. Met. Hard Mater. 80 (2019) 40–68.
[5] J.J. Roa, E. Jiménez-Piqué, J.M. Tarragó, D.A. Sandoval, A. Mateo, J. Fair, L. Llanes, Mater. Sci. Eng. A 676 (2016) 487–491.
[6] B. Roebuck, Int. J. Refract. Met. Hard Mater. 24 (2006) 101–108.
[7] H. Engqvist, S. Jacobson, N. Axén, Wear 252 (2002) 384–393.
[8] K.S. Ravichandran, Acta Metall. Mater. 42 (1994) 143–150.
[9] K.P. Mingard, B. Roebuck, E.G. Bennett, M.G. Gee, H. Nordenstrom, G. Sweetman, P. Chan, Int. J. Refract. Met. Hard Mater. 27 (2009) 213–223.
[10] J. Jeppsson, K. Mannesson, A. Borgenstam, J. Ågren, Acta Mater. 59 (2011) 874–882.
[11] I. Borgh, P. Hedström, J. Odqvist, A. Borgenstam, J. Ågren, A. Gholinia, B. Winiarski, P.J. Withers, G.E. Thompson, K. Mingard, M.G. Gee, Acta Mater. 61 (2013) 4726–4733.
[12] S.M. He, N.H. Van Dijk, M. Paladugu, H. Schut, J. Kohlbrecher, F.D. Tichelaar, S. Van Der Zwaag, Phys. Rev. B: Condens. Matter Mater. Phys. 82 (2010) 174111.
[13] A. Deschamps, F. De Geuser, J. Appl. Crystallogr. 44 (2011) 343–352.
[14] M. Bischof, S. Mayer, H. Leitner, H. Clemens, P. Staron, E. Geiger, A. Voiticek, W. Knabl, Int. J. Refract. Met. Hard Mater. 24 (2006) 437–444.
[15] R.N. Andrews, J. Serio, G. Muralidharan, J. Ilavsky, J. Appl. Crystallogr. 50 (2017) 734–740.
[16] V. Ryukhtin, J. Šaroun, S. Harjo, Y. Motohashi, M. Baron, R. Loidl, J. Appl. Crystallogr. 36 (2003) 478–483.
[17] ASTM International, B330 - 15 Standard Test Methods for Estimating Average Particle Size of Metal Powders and Related Compounds Using Air Permeability, 2015.
[18] P. Strunz, J. Saroun, P. Mikula, F. Eichhorn, J. Appl. Crystallogr. 30 (1997) 844–848.
[19] F. Bachmann, R. Hielscher, H. Schaeben, Ultramicroscopy 111 (2011) 1720–1733.
[20] S. Lay, S. Hamar-Thibault, M. Loubradou, Interface Sci. 12 (2004) 187–195.
[21] J. Šaroun, J. Appl. Crystallogr. 33 (2000) 824–828.
[22] O. Glatter, J. Appl. Crystallogr. 13 (1980) 7–11.
[23] J. Weidow, S. Norgren, H.-O. Andrén, Int. J. Refract. Met. Hard Mater. 27 (2009) 817–822.
[24] J. Weidow, H.-O. Andrén, Acta Mater. 58 (2010) 3888–3894.
[25] M. Walbrühl, D. Linder, J. Ågren, A. Borgenstam, Int. J. Refract. Met. Hard Mater. 68 (2017) 41–48.
[26] J.O. Andersson, T. Helander, L. Höglund, P. Shi, B. Sundman, Calphad 26 (2002) 273–312.
[27] I. Borgh, P. Hedström, T. Persson, S. Norgren, A. Borgenstam, J. Ågren, J. Odqvist, Int. J. Refract. Met. Hard Mater. 43 (2014) 205–211.
[28] J. Gurland, Trans. Metall. Soc. AIME 212 (1958) 452–460.
[29] E.E. Underwood, Microstruct. Anal, Springer US, Boston, MA, 1973 35–66.
[30] ASTM International, ASTM E112-13 Standard Test Methods for Determining Average Grain Size, 2013.